

Molecular Structures of Free-Base Corroles: Nonplanarity, Chirality, and Enantiomerization

Jan Capar,^a Jeanet Conradie,^{a,b} Christine M. Beavers^c and Abhik Ghosh^{*,a}

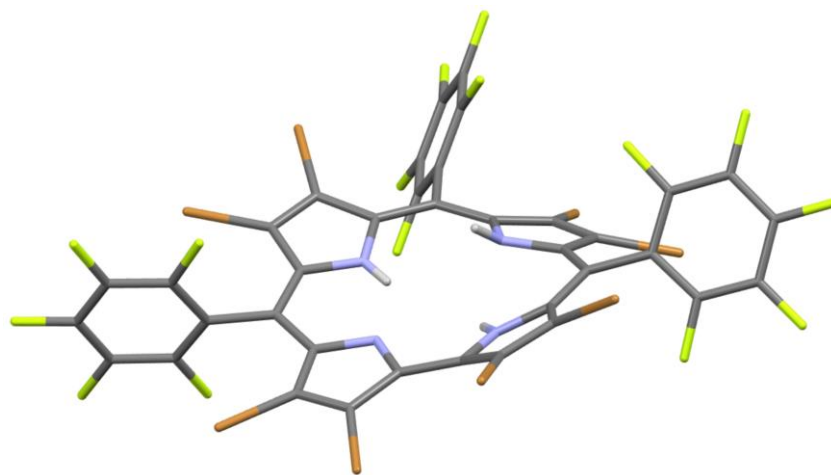
^aDepartment of Chemistry and Center for Theoretical and Computational Chemistry

University of Tromsø, 9037 Tromsø, Norway; Email: abhik@chem.uit.no;

^bDepartment of Chemistry, University of the Free State, 9300 Bloemfontein,
Republic of South Africa

^cAdvanced Light Source, Lawrence Berkeley National Laboratory, Berkeley,
CA, USA

TOC graphic:

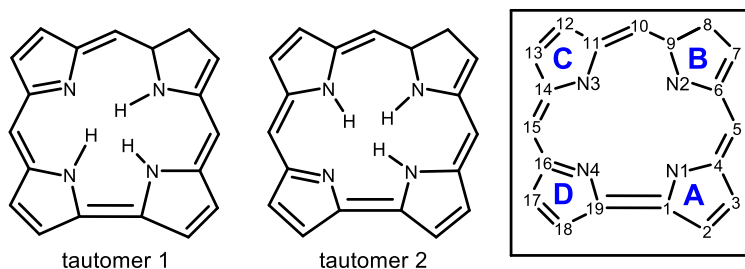


Abstract. The molecular structures of free-base corroles are illustrative of a variety of bonded and nonbonded interactions including aromaticity, intra- as well as inter-molecular hydrogen bonding, steric interactions among multiple NH hydrogens within a congested central cavity, and the effects of peripheral substituents. Against this backdrop, an X-ray structure of 2,3,7,8,12,13,17,18-octabromo-5,10,15-tris(pentafluorophenyl)corrole, $H_3[Br_8TPFPCor]$, corresponding to a specific tautomer, has been found to exhibit the strongest nonplanar distortions observed to date for any free-base corrole structure. Two adjacent *N*-protonated pyrrole rings are tilted with respect to each other by approximately 97.7° , while the remainder of the molecule is comparatively planar. Dispersion-corrected DFT calculations were undertaken to investigate to what extent the strong nonplanar distortions can be attributed to steric effects of the peripheral substituents. For *meso*-triphenylcorrole, DFT calculations revealed nonplanar distortions that are only marginally less pronounced than those found for $H_3(Br_8TPFPCor)$. A survey of X-ray structures of sterically unhindered corroles also uncovered additional examples of rather strong nonplanar distortions. Detailed potential energy calculations as a function of different saddling dihedrals also emphasized the softness of the distortions. Because of nonplanar distortions, free-base corrole structures are chiral. For $H_3[Br_8TPFPCor]$, DFT calculations led to an estimate of 15 kcal/mol (0.67 eV) as the activation barrier for enantiomerization of the free-base structures, which is significantly higher than the barrier for NH tautomerism calculated for this molecule, about 5 kcal/mol (0.2 eV). In summary, steric crowding of the internal NH hydrogens appears to provide the main driving force for nonplanar distortions of *meso*-triarylcorroles; the presence of additional β -substituents adds marginally to this impetus.

Introduction. As fully aromatic versions of the corrin ring of B₁₂ cofactors, corroles are superficially similar to porphyrins, yet a closer look reveals several important differences. Perhaps the most obvious difference is that, free-base porphyrins are diprotic ligands, whereas corroles are triprotic (Scheme 1). Corroles also lack one *meso*-carbon and their central, metal-binding cavity is accordingly more constricted than that of porphyrins. As tightly binding, trianionic ligands, corroles give rise to many stable higher-valent transition metal complexes; some of these may be described as noninnocent.¹ Corroles also differ from porphyrins in terms of their conformational properties.² Porphyrins are much more susceptible to nonplanar distortions such as ruffling or saddling than corroles. The relative rigidity of corroles vis-à-vis nonplanar distortions may be largely related to the direct C₁-C₁₉ linkage, which is resistant to both pyramidalization (which would be required for ruffling) and twisting (which would be required for saddling). Crystallographic and density functional theory (DFT) studies in our laboratory suggest that whereas ruffling is essentially a forbidden distortion mode for corroles, saddling is largely limited to copper corroles.³ The great majority of metallocorroles are either planar or mildly domed, although a few cases of strong doming are also known.⁴

Against this context, the conformations of free-base corroles are of particular interest. As discussed in more detail below, several X-ray structures of *meso*-triarylcorroles are available and these evince significant out-of-plane tilting of one of the *N*-protonated pyrrole rings. Little exact information, however, is available on sterically encumbered, undecasubstituted free-base corroles. Thus, the central hydrogens of a free-base undecaarylcorrole were found to be disordered. This was also the case in a low-resolution X-ray structure of the important ligand 2,3,7,8,12,13,17,18-octabromo-5,10,15-tris(pentafluorophenyl)corrole, H₃[Br₈TPFPCor].⁵ Despite the low resolution, the latter structure revealed a dramatically nonplanar corrole macrocycle. In this study, we report a high-resolution X-ray structure of H₃[Br₈TPFPCor] that corresponds to a given tautomer (tautomer 2 in the notation of Scheme 1).

Encouraged by this successful structure determination, we conducted a thorough DFT study of nonplanar distortion potentials of free-base corroles. One noteworthy point is that the nonplanar conformations of free-base corroles are chiral. Accordingly, we also made an attempt to determine energy barriers associated with enantiomerization. The DFT studies nicely complement the existing experimental data on free-base corroles and shed light on the conformational characteristics of corroles relative to porphyrins.



Scheme 1. The two possible tautomers of the free base corrole and the numbering scheme used.

Methods. Free-base $H_3[Br_8TPFPC]$ was prepared as reported earlier and recrystallized from CH_2Cl_2/n -hexane solution by slow evaporation technique. Dark green shard of dimensions $0.140 \times 0.080 \times 0.060 \text{ mm}^3$ was mounted in the 100(2) K nitrogen cold stream provided by a Oxford Cryosystems Cryostream 700 Plus low temperature apparatus on the goniometer head of a Bruker D8 diffractometer equipped with a ApexII CCD detector on beamline 11.3.1 at the Advanced Light Source in Berkeley, CA. Diffraction data were collected using synchrotron radiation monochromated using silicon(111) to a wavelength of $0.6199(1) \text{ \AA}$. An approximate full sphere of data to $2\theta_{\text{max}} = 67^\circ$ was collected using $0.3^\circ \omega$ scans. The data were integrated using the program SAINT v7.68A. A multi-scan correction for absorption was applied using the program SADABS-2008/1. A total of 128423 reflections were collected, of which 24101 were unique [$R(\text{int}) = 0.0818$], and 17064 were observed [$I > 2\sigma(I)$]. The structure was solved by dual-space methods (SHELXT) and refined by full-matrix least-squares on F^2 (SHELXL-2014) using 616 parameters and one restraint for the disordered solvent. The hydrogen atoms on the pyrrole nitrogens were generated geometrically after careful analysis of the bonding environment, then subsequently allowed to refine freely. The hydrogen atoms on the disordered dichloromethane molecule were generated geometrically and refined as riding atoms with $C-H = 0.95-0.99 \text{ \AA}$ and $U_{\text{iso}}(H) = 1.2 \text{ times } U_{\text{eq}}(C)$. The maximum and minimum peaks in the final difference Fourier map were 1.705 and $-1.619 \text{ e.\AA}^{-3}$. This residual density lies very close to the bromine atoms, and possibly corresponds to slight bromine disorder. Additional information is given in Table 1 and in the cif file included as Supporting Information.

All DFT calculations were carried out with the BP86⁶ exchange-correlation functional, augmented with Grimme's dispersion corrections D,⁷ STO-TZP basis sets, and a suitably fine grid for numerical integration of matrix elements and tight convergence criteria for both SCF and geometry iterations, as implemented in the ADF program system.⁸

Table 1. Crystal data for H₃[Br₈TPFPC].

Sample	H ₃ [Br ₈ TPFPC]
Chemical formula	C ₃₇ H ₃ N ₄ F ₁₅ Br ₈ 0.5(CH ₂ Cl ₂)
Formula mass	1470.18
Crystal system	monoclinic
Space group	<i>C2/c</i>
λ (Å)	0.6199
a (Å)	21.7652(8)
b (Å)	20.7937(8)
c (Å)	17.9564(7)
α (°)	90
β (°)	95.343(2)
γ (°)	90
Z	8
V (Å ³)	8091.4(5)
Temperature (K)	100(2)
Density (g/cm ³)	2.414
Measured reflections	24101
Unique reflections	17064
Parameters	616
Restraints	1
R_{int} (%)	8.18
θ range (°)	1.184 – 33.060
R_1, wR_2 all data	0.0700, 0.1416
R_1, wR_2 [$I > 2\sigma(I)$]	0.0452, 0.1235
S (GooF) all data	1.032
Max/min res. Dens. (e/Å ³)	1.694/-1.626

Results and discussion. Figure 1 presents highlights of the BP86-D/TZP optimized geometries of the two tautomers of unsubstituted free-base corrole. Figure 2 presents similar data for the *meso*-triarylcorroles H₃[TPCor] and H₃[TPFPCor], as well as corresponding experimental data derived from X-ray crystal structures. For all free-base corroles examined, the two tautomers were found to be almost perfectly equienergetic, i.e. to within 0.05 eV. Table 1 lists the so-called ‘saddling dihedrals’ for the various optimized structures. As far as nonplanar distortions are concerned, the main lesson from these results is that, regardless of the tautomeric structure, the saddling dihedral (χ_1) involving pyrrole rings A and B is the highest ($> 55^\circ$), provided the nitrogens in both rings are protonated. The other saddling dihedrals are generally much smaller. A comparison of Figures 1 and 2 also indicate that the free-base *meso*-triarylcorroles exhibit somewhat higher saddling dihedrals than the as yet experimentally unknown parent corrole.

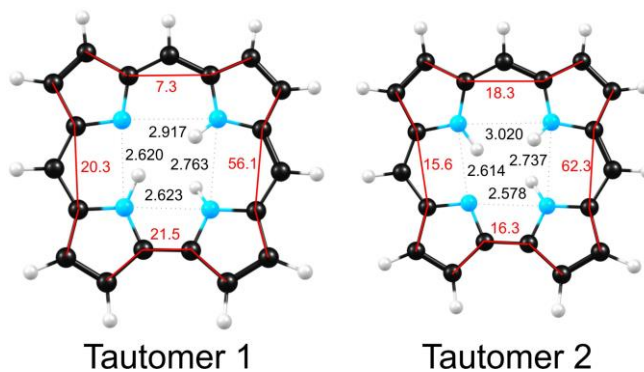


Figure 2. BP86-D/TZP optimized structure of the two tautomers of the unsubstituted free base corrole, H₃[Cor]. Distances (Å) are shown in black and corrole saddling dihedrals in red (°). Color code of atoms (online version): C (black), N (blue), H (white).

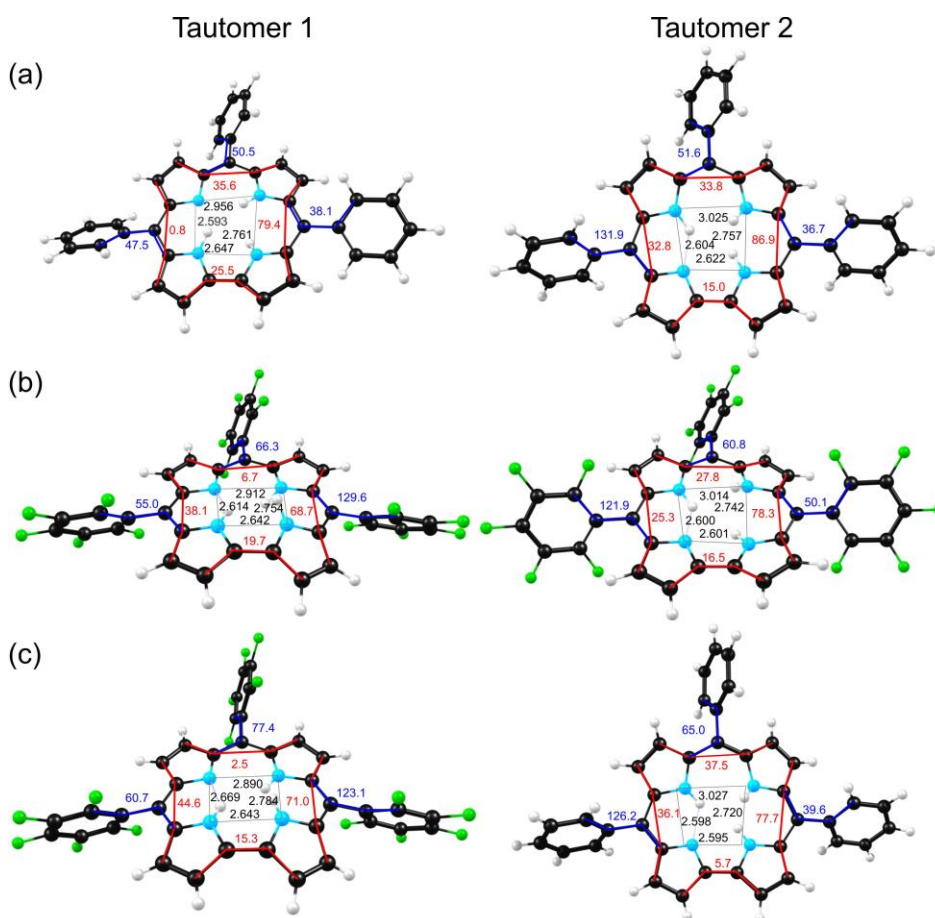


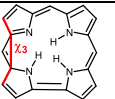
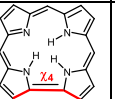
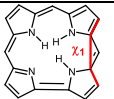

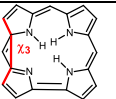



Figure 3. BP86-D/TZP calculated (a) H₃[TPFCor] and (b) H₃[TPFPCor] and (c) experimental structures H₃[TPFPCor] (left) [9] and H₃[TPFCor] (right) [9]. Distances (Å) are shown in black, corrole saddling dihedrals in red (°) and corrole-aryl dihedrals (°) in blue. Color code of atoms (online version): C (black), N (blue), H (white), F (green).

Table 1. Saddling dihedrals ($^{\circ}$) for BP86-D/TZP optimized structures.

	Tautomer 1				Tautomer 2			
								
H ₃ [Cor]	56.1	7.3	30.2	21.5	62.3	18.3	15.6	16.3
H ₃ [TPFPCor]	68.7	6.7	38.1	19.7	78.3	27.8	25.3	16.5
H ₃ [TPCor]	79.4	35.6	0.8	25.5	86.9	33.8	32.8	15.0
H ₃ [Br ₈ TPFPCor]	85.9	37.8	7.8	39.0	93.8	47.4	14.0	37.4
H ₃ [Br ₈ TPCor]	100.4	55.5	23.3	44.2	106.3	60.3	25.4	42.2

Against this context, the experimental molecular structure of tautomer 2 of H₃(Br₈TPFPCor) is extremely distorted (Figures 4 and 5). The χ_1 dihedral is 97.7° , the highest for the nearly 22 or so high-resolution free-base corrole structures reported to date. In other words, pyrrole rings A and B are essentially orthogonal to each other, a remarkable distortion for an aromatic compound. As shown in Figure 6, the NH unit in ring B engages in hydrogen bonding with a meta-F of a pentafluorophenyl group of an adjacent corrole molecule. Such intermolecular hydrogen bonding has been commonly observed for free-base corroles.

To what extent can the remarkable distortion of the χ_1 dihedral be attributed to steric effects of the peripheral substituents? To answer this question, as well as to obtain a general idea of the energetics of nonplanar distortion of free-base corroles, we carried out potential energy scans as a function of the various saddling dihedrals for both tautomers of five corroles – H₃[Cor], H₃[TPCor], H₃[TPFPCor], H₃[Br₈TPCor], and H₃[Br₈TPFPCor]. Figure 7 depicts the potential energy curve associated with the saddling dihedral χ_2 . Based on these results, we are led to conclude that, regardless of the specific system, distortions of $\pm 20^{\circ}$ of the dihedrals χ_1 or χ_2 relative to their equilibrium values cost only about 0.05 eV or 1 kcal/mol. Indeed, according to Table 1, the optimized saddling dihedrals of the sterically unhindered corrole H₃[TPCor] are not particularly different from that of H₃[Br₈TPFPCor]. A literature survey of saddling dihedrals in free-base corrole structures (where the tautomeric form is clearly assignable), summarized in Table 2, also revealed a handful of sterically unhindered free-base corroles with nonplanar distortions just slightly lower than that observed for H₃[Br₈TPFPCor] in this study.

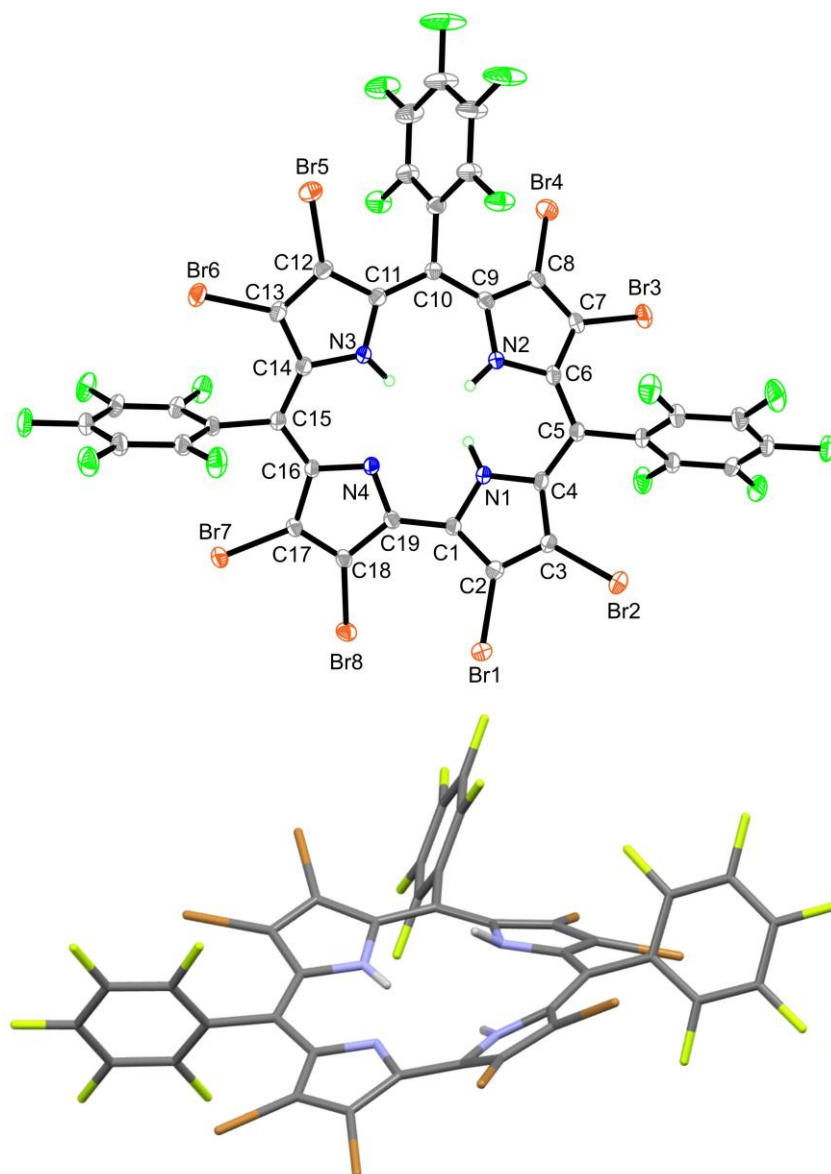


Figure 4. Two views of the X-ray structure of H₃[Br₃TPFPC]: thermal ellipsoid plot (top) and wireframe side view (bottom).

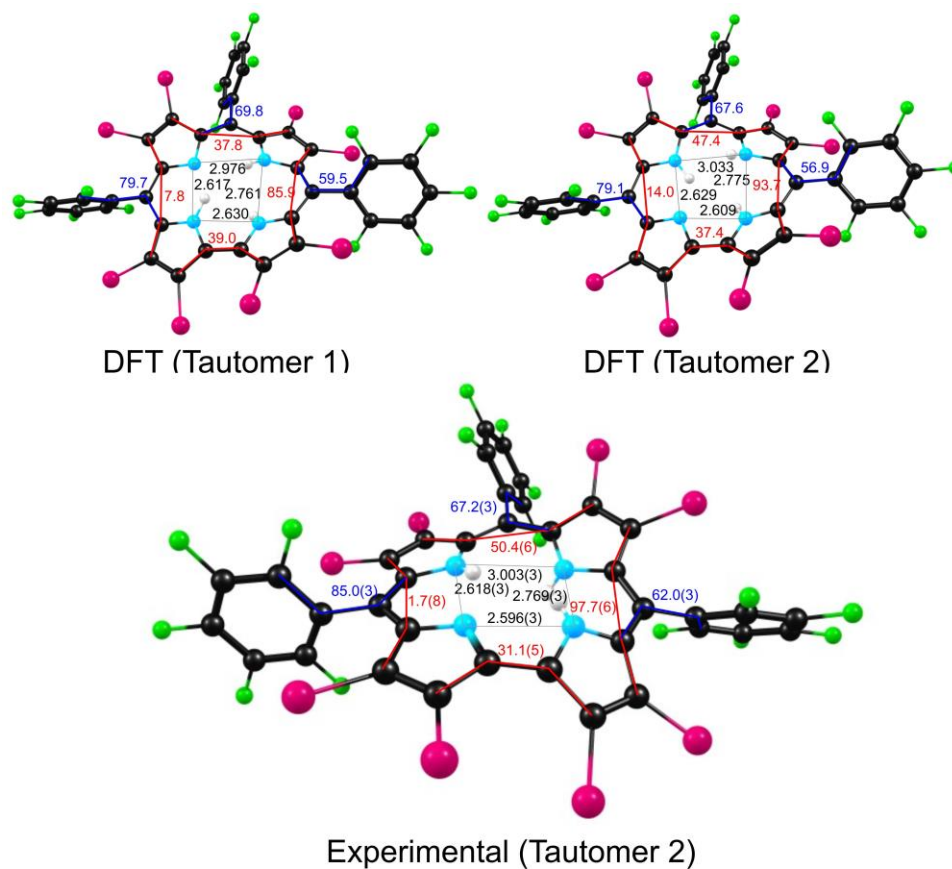


Figure 5. Experimental and BP86-D/TZP optimized $H_3[Br_8TPFPCor]$. Distances (\AA) are shown in black, corrole saddling dihedrals in red ($^\circ$) and corrole-aryl dihedrals ($^\circ$) in blue. Color code of atoms (online version): C (black), N (blue), H (white), F (green), Br (red).

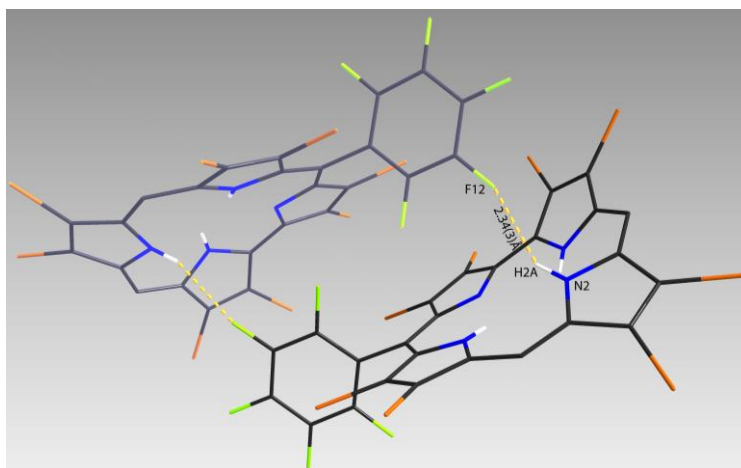


Figure 6. N-H \cdots F-C hydrogen bonding interactions in solid $H_3[Br_8TPFPCor]$.

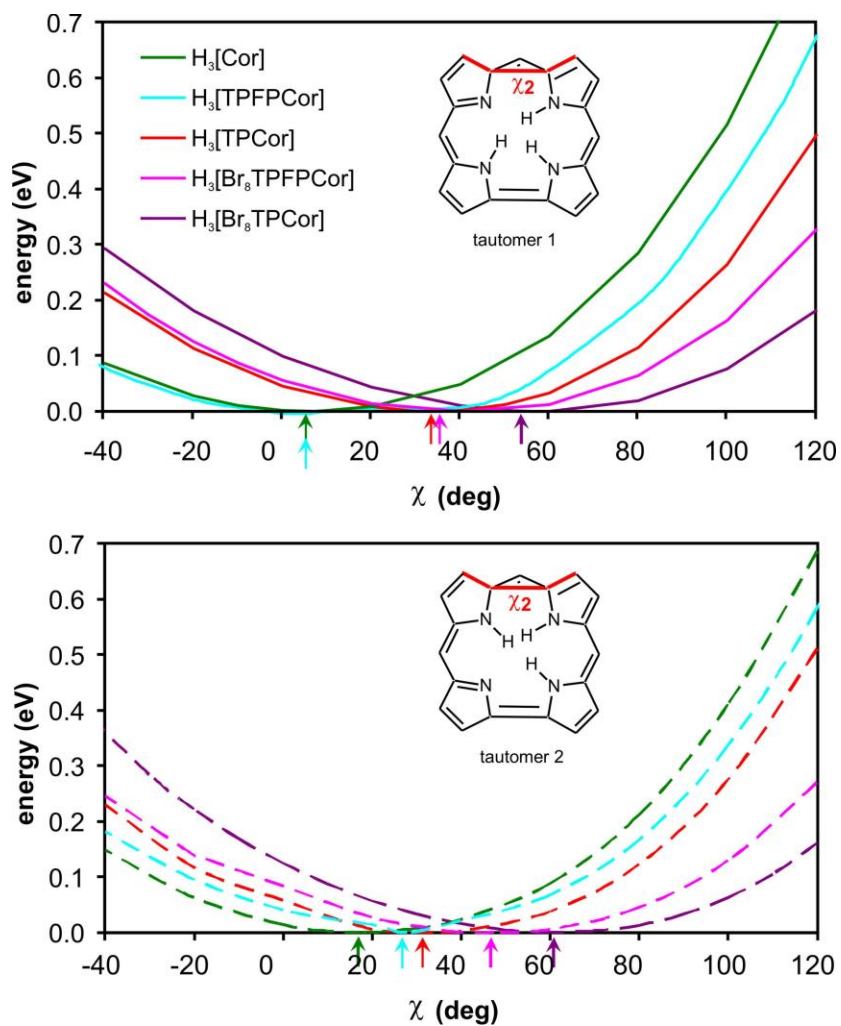


Figure 7. Saddling PE curves as a function of the dihedral indicated (calculated with BP86-D). The solid (top graph) and dotted (bottom graph) lines give the curves for tautomer 1 and 2 respectively. Arrows indicate the minima of the different curves.

Table 2. Saddling dihedrals in X-ray structures of free-base corroles.

Compound	Tautomer	χ_1	χ_2	χ_3	χ_4	CSD	ref
5,5',10,10',15,15'-Hexakis(pentafluorophenyl)-3,3'-bicorrole, 1,4-dioxane and <i>n</i> -octane solvate (dimer)	1	61.8	6.1	21.3	29.8	BATKUE	[10]
	1	68.8	11.6	21.3	25.8		
2-(4,4,5,5-Tetramethyl-(1,3,2)-dioxaborolan-2-yl)-5,10,15-tris(pentafluorophenyl)corrole	1	64.8	10.4	37.5	22.6	CAYZUY	[11]
5,15-Bis(trifluoromethyl)-10-(pentafluorophenyl)corrole	1	64.1	21.7	22.1	14.1	GIBXOF	[12]
5,10,15-Tris(pentafluorophenyl)corrole, ethyl acetate solvate	1	71.0	2.5	44.6	15.3	JEFBIG	[9]
5,15-Bis(pentafluorophenyl)-10-(3-vinylphenyl)corrole	1	59.7	36.8	27.5	11.9	KUHWOA	[13]
2,3,17-Tribromo-5,10,15-tris(pentafluorophenyl)corrole	1	2.3	20.5	73.6	23.4	MULNUD	[14]
5,10,15-Tris(pentafluorophenyl)corrole, chloroform solvate	1	67.8	14.1	28.3	21.1	UCUPOZ	[15]
5,10,15-Tris(perfluorophenyl)corrole, <i>m</i> -xylene solvate	1	67.3	14.6	20.0	19.1	UHEWOT	[16]
10-(4-(5-Carboxy-2,7-di- <i>t</i> -butyl-9,9-dimethylxanthene))-5,15-bis(pentafluorophenyl)corrole, <i>n</i> -hexane solvate	1	71.6	20.2	24.1	24.4	UWOCEP	[17]
5,15-Bis(pentafluorophenyl)-10-(2-thienyl)corrole	1	74.4	40.6	8.2	18.1	VAJMAW	[18]
5,10,15-Tris(2,6-difluorophenyl)corrole	1	70.5	15.6	27.4	18.4	XAVBUT	[19]
5,10,15-Triphenylcorrole, methanol solvate	2	55.6	42.0	34.2	20.0	ELAGIH	[20]
5,10,15-Triphenylcorrole	2	77.7	37.5	36.1	5.8	JEFBEC	[9]
2-Bromo-5,10,15-tri- <i>p</i> -tolylcorrole, chloroform solvate	2	88.7	26.5	43.1	13.7	MAJMOB	[21]
18-Nitro-5,10,15-tris(4-methylphenyl)corrole, chloroform solvate	2	80.4	34.6	0.3	18.9	QEJPIG	[22]
5,10,15-Tris(heptafluoropropyl)corrole	2	63.6	31.7	15.9	9.8	QORBII	[23]
10-(4-(5-Methoxycarbonyl-2,7-di- <i>t</i> -butyl-9,9-dimethylxanthene))-5,15-bis(4- <i>t</i> -butylphenyl)corrole, <i>n</i> -hexane solvate	2	20.4	6.2	60.8	23.5	UWOCAL	[17]
3-Formyl-5,10,15-triphenylcorrole	2	74.9	30.2	3.5	16.1	XABFIQ	[24]
5,15-Bis(pentafluorophenyl)-10-(4-methoxyphenyl)corrole, <i>n</i> -hexane solvate (two molecules in asymmetric unit)	2	74.4	31.5	23.8	13.8	XAVBON	[19]
	2	73.9	26.7	7.8	20.9		

An intriguing topological property of corrole tautomers is their chirality. Given the strong nonplanar distortions exhibited by some of them, an interesting point concerns the energetics of enantiomerization, which we investigated via a series of constrained geometry optimizations as a function of the dihedral χ'_1 shown in Figure 7. The equilibrium value of this dihedral is approximately 31° and only when the value has reached nearly -29° does the ring system suddenly ‘invert’ and become the other enantiomer. Although a true transition state could not be optimized for this process (a somewhat challenging exercise in view of the size of the system), an activation barrier of about 0.67 eV (15 kcal/mol) may be inferred from Figure 7. A barrier of this magnitude is consistent with the potential isolation, such as via cocrystallization with an enantiopure chiral additive, of a given enantiomer of a free-base corrole.

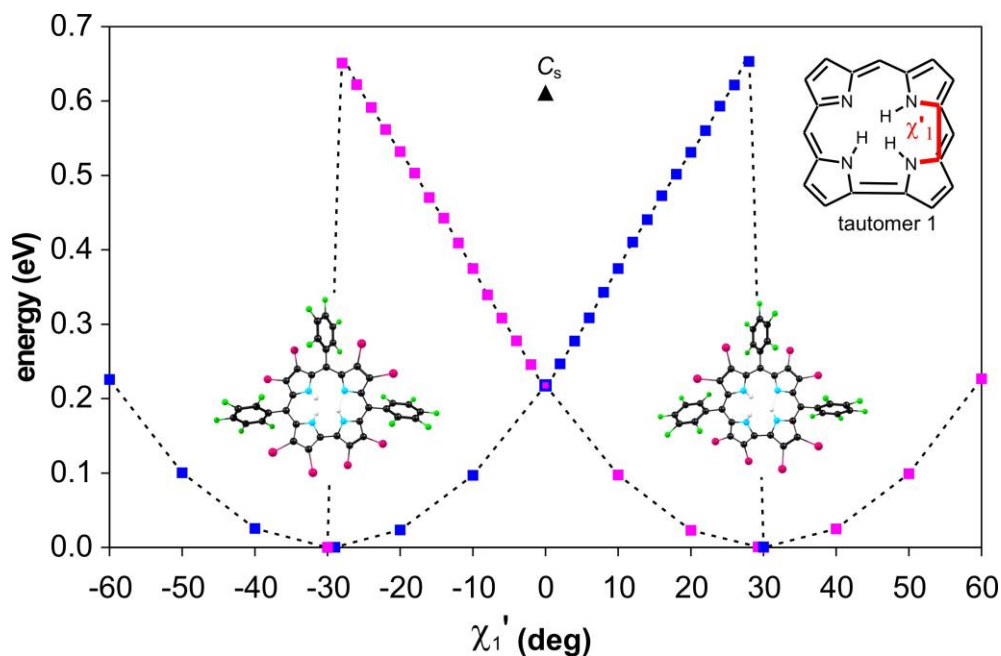


Figure 7. Potential energy curves for tautomer 1 of $H_3[Br_8TPFPCor]$ as a function of the dihedral indicated (calculated with BP86-D), with all other internal coordinates optimized. The opti= +29° (right). Note the abrupt drop in energy at χ_1' approximately equal to $\pm 29^\circ$. The energy of a planar C_s conformation is indicated by a black triangle.

Conclusions. The molecular structures of free-base corroles are determined by a complex interplay of aromaticity, steric interactions between multiple NH hydrogens within a congested central cavity, the effects of peripheral substituents, and both intra- and inter-molecular hydrogen bonding. Against this context, an X-ray structure of the important ligand 2,3,7,8,12,13,17,18-octabromo-5,10,15-tris(pentafluoro-phenyl)corrole, $H_3[Br_8TPFPCor]$, corresponding to a specific tautomer, has been found to exhibit the strongest nonplanar distortions observed to date for any free-base corrole. Two adjacent *N*-protonated pyrrole rings are tilted with respect to each other by approximately 97.7° , whereas the remainder of the molecule is comparatively planar. Interestingly, both X-ray structural data and DFT calculations indicate that the nonplanar distortions of certain sterically unhindered free-base triarylcorroles are only slightly less pronounced than those observed for $H_3[Br_8TPFPCor]$. Steric repulsion among the internal NH hydrogens thus appears to provide the key driving force for nonplanar distortions of *meso*-triarylcorroles; the presence of additional β -substituents adds marginally to this impetus.

Acknowledgement. This work was supported by the Research Council of Norway (A.G.) and the South African National Research Foundation (J.C.). The Advanced Light Source is supported by the Director, Office of Science, Office of Basic Energy Sciences, of the U.S. Department of Energy under Contract No. DE-AC02-05CH11231.

References

1. Palmer, J.H. *Transition Metal Corrole Coordination Chemistry*. in: *Molecular electronic structures of transition metal complexes I. Structure and Bonding*. No.142; Springer-Verlag: Berlin, Heidelberg, 2012; pp 49-89.
2. Thomas, K.E.; Conradie, J.; Hansen, L-K.; Ghosh, A. *Inorg. Chem.* **2011**, *50*, 3247-3251.
3. (a) Thomas, K.E.; Conradie, J.; Hansen, L-K.; Ghosh, A. *Eur. J. Inorg. Chem.* **2011**, *12*, 1865-1870. (b) Thomas, K.E.; Alemayehu, A.B.; Conradie, J.; Beavers, C.M.; Ghosh, A. *Inorg. Chem.* **2011**, *50*, 12844–12851.
4. Thomas, K.E.; Alemayehu, A.B.; Conradie, J.; Beavers, C.M.; Ghosh, A. *Accounts of Chemical Research* **2012**, *45*, 1203–1214.
5. Capar, C.; Hansen, L-K.; Conradie, J.; Ghosh, A. *J. Porphyrins Phthalocyanines* **2010**, *14*: 509-512.
6. (a) Becke, A.D. *Phys. Rev.* **1988**, *A38*, 3098-3100. (b) Perdew, J.P. *Phys. Rev.* **1986**, *B33*, 8822-8824; Erratum: Perdew, J.P. *Phys. Rev.* **1986**, *B34*, 7406.
7. Grimme, S. *J. Comput. Chem.* **2006**, *27*, 1787-1799.
8. Van Gisbergen, S.J.A. Amsterdam Density Functional molecular modelling suite. May be obtained from: Scientific Computing & Modelling NV, Division of Theoretical Chemistry, Vrije Universiteit, De Boelelaan 1083, Amsterdam 1081 HV, The Netherlands; www.scm.com.
9. Ding, T.; Harvey, J.D.; Ziegler, C.J. *J. Por. Phth.* **2005**, *9*, 22-27.
10. Hirabayashi, S.; Omote, M.; Aratani, N.; Osuka, A. *Bull. Chem. Soc. Jpn.* **2012**, *85*, 558-562.
11. Hiroto, S.; Hisaki, I.; Shinokubo, H.; Osuka, A. *Angew. Chem., Int. Ed.* **2005**, *44*, 6763–6766.
12. Goldschmidt, R.; Goldberg, I.; Balazs, Y.; Gross, Z. *J. Por. Phth.* **2006**, *10*, 76-86.
13. Kim, K.; Kim, I.; Maiti, N.; Kwon, S.J.; Bucella, D.; Egorova, O.A.; Lee, Y.S.; Kwak, J.; Churchill, D.G. *Polyhedron* **2009**, *28*, 2418–2430.
14. Du, R.-B.; Liu, C.; Shen, D.-M.; Chen, Q.-Y. *Synlett*, **2009**, 2701-2705.

-
15. Reith L.; Stiftinger M.; Monkowius U.; Knör G.; Schöfberger W. *Inorg. Chem.* **2011**, *50*, 6788–6797.
16. Gross, Z.; Galili, N.; Simkhovich, L.; Saltsman, I.; Botoshansky, M.; Blaser, D.; Boese, R.; Goldberg, I. *Org. Lett.* **1999**, *1*, 599–602.
17. Dogutan, D. K.; Stoian, S. A.; McGuire, R. Jr.; Schwalbe, M.; Teets, T. S.; Nocera, D. G. *J. Am. Chem. Soc.* **2011**, *133*, 131–140.
- 18 Egorova, O. A.; Tsay, O. G.; Khatua, S.; Meka, B.; Maiti, N.; Kim, M.-K.; Kwon, S. J.; Huh, J. O.; Bucella, D.; Kang, S.-O.; Kwak, J.; Churchill, D. G. *Inorg. Chem.* **2010**, *49*, 502–512.
- 19 Kumar, A.; Goldberg, I.; Botoshansky, M.; Buchman, Y.; Gross, Z. *J. Am. Chem. Soc.* **2010**, *132*, 15233–15245.
- 20 Paolesse, R.; Marini, A.; Nardis, S.; Froiio, A.; Mandoj, F.; Nurco, D. J.; Prodi, L.; Montalti, M.; Smith, K.M. *J. Porphyrins Phthalocyanines* **2003**, *7*, 25-36.
- 21 Nardis, S.; Pomarico, G.; Mandoj, F.; Fronczek, F.R.; Smith, K.M.; Paolesse, R. *J. Porphyrins Phthalocyanines* **2010**, *14*, 752-758.
- 22 Stefanelli, M.; Pomarico, G.; Tortora, L.; Nardis, S.; Fronczek, F. R.; McCandless, G. T.; Smith, K. M.; Manowong, M.; Fang, Y.; Chen, P.; Kadish, K. M.; Rosa, A.; Ricciardi, G.; Paolesse, R. *Inorg. Chem.* **2012**, *51*, 6928–6942.
- 23 Simkhovich, L.; Goldberg, I.; Gross, Z. *J. Inorg. Biochem.* **2000**, *80*, 235-238.
- 24 Paolesse, R.; Nardis, S.; Venanzi, M.; Mastroianni, M.; Russo, M.; Fronczek, F. R.; Vicente, M. G. H. *Chem.-Eur. J.* **2003**, *9*, 1192–1197.